

Nonequilibrium Spin Transport on Au(111) Surfaces

Ming-Hao Liu, Son-Hsien Chen, and Ching-Ray Chang

Department of Physics, National Taiwan University, Taipei 10617, Taiwan

(Dated: April 13, 2019)

The well-known experimentally observed sp -derived Au(111) Shockley surface states with Rashba spin splitting are perfectly fit by an effective tight-binding model with simplest considerations: p_z -orbital and nearest neighbor hopping. The extracted band parameters are then imported to perform the Landauer-Keldysh formalism to calculate the nonequilibrium spin transport in a two-terminal setup sandwiching a Au(111) surface channel. Obtained results stand on an experimental footing and demonstrate (i) intrinsic spin-Hall effect, (ii) current-induced spin polarization, and (iii) Rashba spin precession, all of which have been experimentally observed in semiconductor heterostructures, but not in metallic surface states. We therefore urge experiments in the latter for these spin phenomena.

PACS numbers: 73.20.At, 73.23.-b, 71.70.Ej

Two-dimensional electron gas (2DEG) is known to exist in two distinct systems: semiconductor heterostructures [1] and metallic surface states [2]. Due to the lack of inversion symmetry introduced by the interface/surface, the spin degeneracy, as the combining consequence of the time reversal symmetry (Kramers degeneracy) and the inversion symmetry, is removed and the energy dispersion becomes spin-split. In semiconductor heterostructures, one of the underlying mechanisms leading to such spin splitting is known as the Rashba spin-orbit coupling [3], which stimulates a series of discussion on plenty of intriguing spin-dependent phenomena. Popular and well-known phenomena include spin precession [4, 5], spin-Hall effect (SHE) [6, 7], and current-induced spin polarization (CISP) [7, 8, 9, 10], all of which have been experimentally observed. Contrarily, none of these in metallic surface states is reported, even though the Rashba effect has been shown to exist therein [11].

To the lowest order in the inplane wave vector k_{\parallel} , the Rashba spin splitting is linear in k_{\parallel} : $\Delta E = E_+ - E_- = \alpha k_{\parallel}$, where the proportional constant α is usually referred to as the Rashba parameter or the Rashba coupling strength. Typical values of α in semiconductor heterostructures are at most of the order of 10^{-2} eV Å [9, 10, 12], while in metallic surface states α can be one or two orders larger.

The first evidence of spin splitting in metallic surface states was pioneered by LaShell *et al.* on Au(111) surfaces at room temperature [13]. The origin of their observed spin splitting was later recognized as the Rashba effect by performing the first-principles electronic-structure and photoemission calculations [14, 15], which are in good agreement with the spin-resolved photoemission experiments [15, 16]. Concluded Rashba parameter is about $\alpha = 0.36$ eV Å. Subsequent findings of giant Rashba spin-orbit coupling is also claimed in Bi(111) surfaces [17] with $\alpha \approx 0.83$ eV Å and in Bi/Ag(111) surface alloy [18] with $\alpha \approx 3.05$ eV Å.

It is therefore legitimate to expect the previously men-

tioned spin-dependent phenomena to be observed on those metallic surfaces with strong Rashba coupling. In this Letter we theoretically study nonequilibrium spin transport in 2DEG held by Au(111) surface states, which exhibit not only strong Rashba coupling but also simple parabola-like dispersions [19]. The latter characteristic allows simplest tight-binding model (TBM) to correctly extract realistic band parameters to be inputted in the nonequilibrium Keldysh Green's function formalism [20], which is recently termed Landauer-Keldysh formalism (LKF) [21, 22].

We first demonstrate that the sp -derived Shockley surface states on Au(111) from Ref. 13 can be well described by an effective TBM [see Fig. 1(a)] for a two-dimensional triangular lattice, taking into account only nearest neighbor hopping and p_z -orbital, subject to the

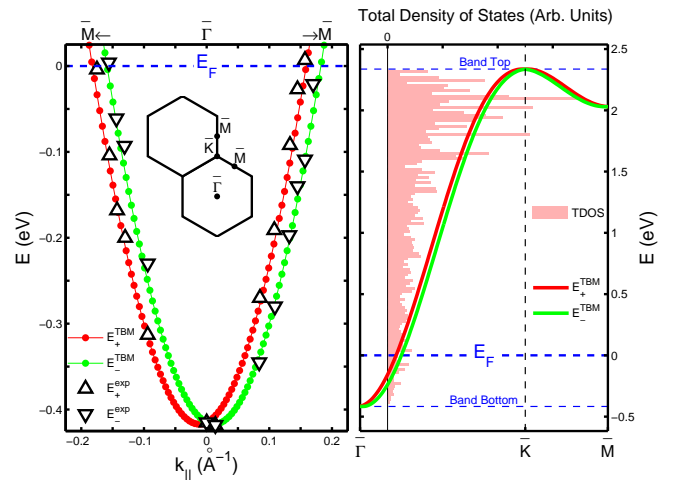


FIG. 1: (Color online) (a) Tight-binding energy dispersion E_{\pm}^{TBM} and the experimentally measured binding energy E_{\pm}^{EXP} of Ref. 13, along the ΓM direction. The surface Brillouin zone is sketched in the inset. (b) Total density of states and E_{\pm}^{TBM} along ΓK and ΓM directions.

Rashba spin splitting. The Hamiltonian matrix reads [23, 24],

$$\mathbb{H} = E_p \mathbb{1} + \sum_{\mathbf{t}_I} e^{i\mathbf{k}_{\parallel} \cdot \mathbf{t}_I} [V_{pp\pi} \mathbb{1} + V_R \mathbf{e}_z \cdot (\vec{\sigma} \times \mathbf{t}_I)], \quad (1)$$

where E_p is the p -orbital energy, \mathbf{t}_I represents the six nearest neighbor hopping vectors, $V_{pp\pi}$ is the band parameter describing the orbital integral under the two-center approximation of Slater and Koster [25], V_R is the Rashba hopping parameter, and $\vec{\sigma} = (\sigma_x, \sigma_y, \sigma_z)$ are the Pauli matrices. The three terms in Eq. (1) are the energy band offset, the kinetic hopping, and the Rashba hopping, respectively. Arranging the two primitive translation vectors for the triangular lattice as $\mathbf{t}_1 = (\sqrt{3}/2, 1/2, 0)a$ and $\mathbf{t}_2 = (-\sqrt{3}/2, 1/2, 0)a$ where a is the lattice constant, the six nearest neighbor hopping vectors are $\mathbf{t}_I = \pm \mathbf{t}_1, \pm \mathbf{t}_2, \pm(\mathbf{t}_1 + \mathbf{t}_2)$, and Eq. (1) then takes the explicit form of

$$\mathbb{H}(\mathbf{k}_{\parallel}) = \begin{pmatrix} E_p + G(\mathbf{k}_{\parallel}) & F(\mathbf{k}_{\parallel}) \\ F^*(\mathbf{k}_{\parallel}) & E_p + G(\mathbf{k}_{\parallel}) \end{pmatrix} \quad (2)$$

with

$$F(\mathbf{k}_{\parallel}) = iV_R[(1 + \sqrt{3}i) \sin \mathbf{k}_{\parallel} \cdot \mathbf{t}_1 + (1 - \sqrt{3}i) \sin \mathbf{k}_{\parallel} \cdot \mathbf{t}_2 + 2 \sin k_y a] \quad (3)$$

$$G(\mathbf{k}_{\parallel}) = 2V_{pp\pi} [2 \cos \frac{\sqrt{3}k_x a}{2} \cos \frac{k_y a}{2} + \cos(k_y a)]. \quad (4)$$

Equation (2) can be diagonalized to yield the energy dispersions

$$E(\mathbf{k}_{\parallel}) = E_p + G(\mathbf{k}_{\parallel}) \pm |F(\mathbf{k}_{\parallel})|. \quad (5)$$

Noting from Eq. (3) that V_R is embedded in $F(\mathbf{k}_{\parallel})$, the above dispersion contains the Rashba term to all (odd) orders in k_{\parallel} .

In the vicinity of $\bar{\Gamma}$, i.e., $|\mathbf{k}_{\parallel}|a \ll 1$, Eqs. (3) and (4) are approximated by $F(\mathbf{k}_{\parallel}) \approx -3V_R(k_x - ik_y)a$ and $G(\mathbf{k}_{\parallel}) \approx 6V_{pp\pi} - (3V_{pp\pi}a^2/2)k_{\parallel}^2$, respectively, and the Hamiltonian matrix (2) then takes the form

$$\mathbb{H}_{k_{\parallel}a \ll 1} = \begin{pmatrix} E_0 - \frac{3V_{pp\pi}a^2}{2}k_{\parallel}^2 & -3V_R(k_x - ik_y)a \\ -3V_R(k_x + ik_y)a & E_0 - \frac{3V_{pp\pi}a^2}{2}k_{\parallel}^2 \end{pmatrix}, \quad (6)$$

where $E_0 \equiv E_p + 6V_{pp\pi}$. Equation (6) is consistent with the p_z -resolved effective Hamiltonian of the earlier TBM by Petersen and Hedegård, who considered all the three p -orbitals, subject to the intra-atomic spin-orbit coupling [26].

We are now in a position to fit our tight-binding dispersion with the experiment of Ref. 13. This can be done by comparing the eigenvalues solved from Eq. (6),

$$E(\mathbf{k}_{\parallel}) \Big|_{ka \ll 1} = E_p + 6V_{pp\pi} - \frac{3V_{pp\pi}a^2}{2}k_{\parallel}^2 \pm 3V_R a |\mathbf{k}_{\parallel}|, \quad (7)$$

with that of the free-electron model, $E(k_{\parallel}) = E_0 + (\hbar^2/2m^*)k_{\parallel}^2 \pm \alpha k_{\parallel}$. In addition to the band offset $E_0 = E_p + 6V_{pp\pi}$, we identify $V_{pp\pi} = -(2/3a^2)(\hbar^2/2m^*)$ and $V_R = \alpha/3a$. The reciprocal vector \mathbf{g}_1 is $(4\pi/\sqrt{3}a)(1/2, \sqrt{3}/2, 0)$. From Ref. 13, we have $\bar{M} = 1.26 \text{ \AA}^{-1}$, $\hbar^2/2m^* \approx 15.2 \text{ eV \AA}^2$, $\alpha \approx 0.3557 \text{ eV \AA}$, and $E_0 \approx -0.415 \text{ eV}$. The norm of \mathbf{g}_1 gives \bar{M} such that the lattice constant is $a = 4\pi/\sqrt{3}|\bar{g}_1| = 5.7581 \text{ \AA}$. Hence we deduce $V_{pp\pi} = -0.3056 \text{ eV}$, $V_R = 0.0206 \text{ eV}$, and $E_p = 1.4188 \text{ eV}$.

Having extracted the band parameters needed in the tight-binding calculation, we show in Fig. 1(a) the perfect consistency between the calculated energy dispersion according to Eqs. (3)–(5) and the experimentally measured binding energy of Ref. 13. Our effective TBM can reproduce the Fermi surface map as well, using again the dispersion (5), but we do not explicitly show. Because of $k_F a \approx 1$ here, k_F being the Fermi wave vector, the low k_{\parallel} approximation form (7), which prescribes two concentric circles in the k_x - k_y plane, provides only a rough description of the Fermi surface. This means that terms with higher order in k_{\parallel} , neglected in Eq. (7), will somewhat contribute, leading to the experimentally measured Fermi surface of the concentric rings slightly distorted from circles [19]. Another important information implied by $k_F a \approx 1$ is that the long wavelength limit, making the electron transport in the lattice free-electron-like and allowing for the finite difference method to apply, is not a good approximation here. Thus the realistic crystal lattice structure of the Au(111) surface has to be taken into account in the nonequilibrium transport calculation by the LKF [27].

In the LKF, the starting point is the second-quantized single particle Hamiltonian [24],

$$\mathcal{H} = \sum_n \varepsilon_n c_n^\dagger c_n + \sum_{\langle m,n \rangle} c_m^\dagger [-t_0 + it_R (\vec{\sigma} \times \mathbf{d}_{mn})_z] c_n, \quad (8)$$

where c_n^\dagger (c_n) is the creation (annihilation) operator of the electron on site n , $\langle m, n \rangle$ means that sites m and n are nearest neighbors to each other, and \mathbf{d}_{mn} is the unit vector pointing from n to m . The correspondence between the Hamiltonians (1) and (8) can be established by setting $\varepsilon_n = E_p$, $-t_0 = V_{pp\pi}$, and $t_R = V_R$. To bridge the gap between the TBM and the LKF, we apply the latter to compute the total density of states (TDOS) for a $80(a\sqrt{3}/2) \times 11a \approx 398.9 \text{ \AA} \times 63.3 \text{ \AA}$ channel made of a Au(111) surface, in perfect contact with two unbiased normal metal leads at the left and right ends of the sample. We will further image the nonequilibrium spin transport on this two-terminal setup later. As shown in Fig. 1(b), the range of the calculated nonvanishing TDOS is consistent with the TBM dispersion along the $\bar{\Gamma}\bar{K}$ direction, which corresponds to the nearest neighbor hopping direction as we considered in the underlying

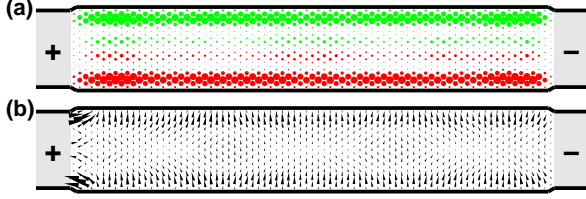


FIG. 2: (Color online) Local spin density of (a) the out-of-plane component $\langle S_z \rangle$ and (b) the inplane component $(\langle S_x \rangle, \langle S_y \rangle)$ in a conducting sample made of Au(111) surface. The size of each local marker depicts the magnitude. In (a), red/dark (green/light) dots denote $\langle S_z \rangle > 0$ ($\langle S_z \rangle < 0$). Both the mean of $|\langle S_z \rangle|$ and $|\langle S_x \rangle, \langle S_y \rangle|$ are of the order of $(\hbar/2) \times 10^{-4}$.

Hamiltonian (8).

Combination of the consistency between the experimental and the TBM dispersions, and that between the dispersion by the TBM and the TDOS by the LKF, indirectly demonstrates that the following imaging of local spin densities by the LKF stands on an experimental footing. As a first demonstration of the nonequilibrium spin transport, we turn on the bias of potential difference $eV_0 = 0.2$ eV between the two normal metal leads. We will denote $\pm eV_0/2$ on the leads by \pm sign. With such injection of an unpolarized electron current, we expect (i) the spin-Hall effect of the intrinsic type, and (ii) the CISP, which follows the Rashba eigenspin direction of the lower energy branch. Both of these can be seen respectively in Figs. 2(a) and 2(b). The former shows an antisymmetric out-of-plane spin accumulation at lateral edges, while the latter shows that the inplane components of spins mostly point to $+y$ axis [28].

Next we inject spin-polarized currents by replacing the left (source) lead with a ferromagnetic electrode. Previously, the self-energy due to the normal metal lead, which is assumed to be semi-infinite, in thermal equilibrium, and in perfect contact with the sample, can be obtained by solving the surface Green's function of the lead [20], subject to Hamiltonian $\mathcal{H}_{\text{lead}} = \mathbf{p}^2/2m + V$. The momentum operator $\mathbf{p} = (p_x, p_y)$ is two-dimensional and the potential describes a infinite potential well of a semi-infinite rectangle shape. The exact form of the lead self-energy reads

$$\Sigma^R(p_1, p_2) = -\frac{2t}{N_d + 1} \sum_{n=1}^{\infty} \sin \frac{n\pi p_1}{N_d + 1} \sin \frac{n\pi p_2}{N_d + 1} \times \frac{e^{ik_n a} \sin(k_n a)}{k_n a} \quad (9)$$

with $k_n a = \sqrt{(E - E_n)/t}$ and $E_n = [n\pi/(N_d + 1)]^2 t$. In Eq. (9), $p_{1(2)} = 1, 2, \dots, N_d$ is the lateral position (in unit of lattice constant a) of the edge site in the sample in contact with the lead, t is the coupling between the sample and the lead and is usually set equal to the kinetic

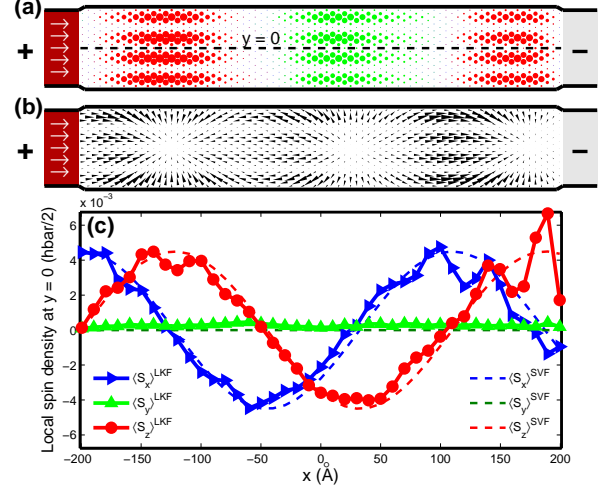


FIG. 3: (Color online) Local spin density of (a) the out-of-plane component $\langle S_z \rangle$ and (b) the inplane component $(\langle S_x \rangle, \langle S_y \rangle)$, in a conducting sample made of Au(111) surface, subject to a ferromagnetic source lead with $+x$ magnetization. (c) $\langle S_x \rangle$, $\langle S_y \rangle$, and $\langle S_z \rangle$ as a function of x at $y = 0$, i.e., along the dashed line sketched in (a). Computed values are compared with the previously obtained spin vector formula based on quantum mechanics.

hopping t_0 in the sample, and $(N_d + 1)a$ is implicitly assumed to be the width of the lead.

To take into account the exchange field inside the ferromagnetic lead, we adopt the Weiss mean field approximation and add a Zeeman term $-\mu_B \vec{\sigma} \cdot \mathbf{B}_{ex}$ ($\mu_B \approx 5.8 \times 10^{-5}$ eV T $^{-1}$ is the Bohr magneton) to $\mathcal{H}_{\text{lead}}$. Typical exchange field may be as high as $|\mathbf{B}_{ex}| \approx 10^{-3}$ T [29], leading to $|\mu_B \mathbf{B}_{ex}| \approx 5.8 \times 10^{-2}$ eV. We will take this value in the forthcoming spin precession demonstration. The explicit form of the self-energy is modified as

$$\Sigma^R(p_1, p_2) = -\frac{2t}{N_d + 1} \sum_{n=1}^{\infty} \sin \frac{n\pi p_1}{N_d + 1} \sin \frac{n\pi p_2}{N_d + 1} \times \sum_{\sigma=\pm} \frac{e^{ik_n^\sigma a} \sin(k_n^\sigma a)}{k_n^\sigma a} |\mathbf{n}\sigma\rangle \langle \mathbf{n}\sigma|, \quad (10)$$

with $k_n^\sigma a = \sqrt{(E - E_n + \sigma |\mu_B \mathbf{B}_{ex}|)/t}$, and $|\mathbf{n}\sigma\rangle$ being the spin-1/2 state ket with quantization axis \mathbf{n} [30]. Note that both Eqs. (9) and (10) are exact without any approximation.

Applying the same voltage difference of 0.2 V and magnetizing the ferromagnetic source lead along $+x$ axis, Figs. 3(a) and 3(b) show the out-of-plane and in-plane components of the local spin densities, respectively. The injected x -polarized spins moving along $+x$ and encountering the Rashba effective magnetic field pointing to $-y$, are forced to precess about $-y$ -axis counterclockwise, and hence the Rashba spin precession is observed. In the free electron model, the

spin precession length (the distance within which the spin completes a precession angle of π) is $L_{so} = (\pi/\alpha)(\hbar^2/2m^*) \approx 134 \text{ \AA}$. Thus the channel length is about 3 times L_{so} , which is consistent to what we observed in Figs. 3(a) and 3(b).

To compare the LKF results with the free electron model in further detail, we recall the spin vector formula based on quantum mechanics [see Eq. (6) of Ref. 31]. Here the spin is initially prepared with $(\theta_s, \phi_s) = (\pi/2, 0)$ and is injected in a Rashba 2DEG along $+x$ direction: $\varphi = \phi = 0$ [φ is defined in Eq. (4) of Ref. 31]. These give $(\langle S_x \rangle, \langle S_y \rangle, \langle S_z \rangle) = (\cos \Delta\theta, 0, \sin \Delta\theta)$ with $\Delta\theta = (2m^*/\hbar^2)\alpha x = 2.34 \times 10^{-2}x$ where x is in unit of \AA . Note that a factor of $\sqrt{3}/2$ responsible for the net and actual hopping distances has to be taken into account in x , since the crystal structure information still exists. Accordingly, good agreement between the LKF and the spin vector formula can be seen in Fig. 3(c).

In conclusion, we have shown that the sp -derived Shockley surface states on Au(111) [13, 14, 15, 16, 19] can be well described by an effective TBM, taking into account p_z -orbital and nearest neighbor hopping only. On-site energy and the hopping parameters required in the LKF calculation can thus be extracted on an experimental footing. The intrinsic SHE and CISP due to injection of unpolarized current, and the Rashba spin precession due to injection of spin-polarized current, are locally imaged by the LKF for a two-terminal setup sandwiching a Au(111) surface channel. Calculated local spin densities in all the three spin phenomena are much stronger than those in semiconductor heterostructures, since the Rashba coupling is one order of magnitude stronger. We therefore suggest experimental measurements for these spin phenomena on Au(111) surfaces and other metallic surface states with strong Rashba coupling such as Bi(111) surfaces [17] or Bi/Ag(111) surface alloy [18]. Another important advantage of these surface states is the applicability of the spin-polarized scanning tunneling microscopy (SPSTM) [32]. Whereas stronger Rashba coupling strengthens the spin signal due to, e.g., the CISP [28], finer structures of the patterns of, e.g., the intrinsic SHE or the spin precession, are also induced. The atomic resolution of the SPSTM may be, compared to the magnetic optical Kerr effect apparatus, a much more promising solution for these measurements.

Financial support of the Republic of China National Science Council Grant No. 95-2112-M-002-044-MY3 is gratefully acknowledged.

-
- [1] John H. Davies, *The Physics of Low-Dimensional Semiconductors* (Cambridge University Press, Cambridge, U.K., 1998).
 [2] S. G. Davison and M. Stešlicka, *Basic Theory of Surface*

- States* (Oxford University Press, Oxford, U.K., 1992).
 [3] E. I. Rashba, *Sov. Phys. Solid State* **2**, 1109 (1960); Yu. A. Bychkov and E. I. Rashba, *JETP Lett.* **39**, 78 (1984).
 [4] J. M. Kikkawa, I. P. Smorchkova, N. Samarth, D. D. Awschalom, *Science* **277**, 1284 (1997).
 [5] Y. Kato, R. C. Myers, A. C. Gossard & D. D. Awschalom, *Nature* **427**, 50 (2003).
 [6] Y. K. Kato, R. C. Myers, A. C. Gossard, D. D. Awschalom, *Science* **306**, 1910 (2004).
 [7] N. P. Stern, S. Ghosh, G. Xiang, M. Zhu, N. Samarth, and D. D. Awschalom, *Phys. Rev. Lett.* **97**, 126603 (2006).
 [8] Y. K. Kato, R. C. Myers, A. C. Gossard, and D. D. Awschalom, *Phys. Rev. Lett.* **93**, 176601 (2004).
 [9] V. Shi, R. C. Myers, Y. K. Kato, W. H. Lau, A. C. Gossard, and D. D. Awschalom, *Nat. Phys.* **1**, 31 (2005).
 [10] C. L. Yang, H. T. He, Lu Ding, L. J. Cui, Y. P. Zeng, J. N. Wang, and W. K. Ge, *Phys. Rev. Lett.* **96**, 186605 (2006).
 [11] G. Bihlmayer, Yu. M. Koroteev, P. M. Echenique, E. V. Chulkov, and S. Blügel, *Surf. Sci.* **600**, 3888 (2006).
 [12] J. Nitta, T. Akazaki, H. Takayanagi, and T. Enoki, *Phys. Rev. Lett.* **78**, 1335 (1997).
 [13] S. LaShell, B. A. McDougall, and E. Jensen, *Phys. Rev. Lett.* **77**, 3419 (1996).
 [14] J. Henk, A. Ernst, and P. Bruno, *Phys. Rev. B* **68**, 165416 (2003).
 [15] J. Henk, M. Hoesch, J. Osterwalder, A. Ernst, and P. Bruno, *J. Phys.: Condens. Matter* **16**, 7581 (2004).
 [16] M. Hoesch, M. Muntwiler, V. N. Petrov, M. Hengsberger, L. Patthey, M. Shi, M. Falub, T. Greber, and J. Osterwalder, *Phys. Rev. B* **69**, 241401(R) (2004).
 [17] Yu. M. Koroteev, G. Bihlmayer, J. E. Gayone, E. V. Chulkov, S. Blügel, P. M. Echenique, and Ph. Hofmann, *Phys. Rev. Lett.* **93**, 046403 (2004).
 [18] Cristian R. Ast, Jürgen Henk, Arthur Ernst, Luca Moreschini, Mihaela C. Falub, Daniela Pacilé, Patric Bruno, Klaus Kern, and Marco Grioni, *Phys. Rev. Lett.* **98**, 186807 (2007).
 [19] Friedrich Reinert, *J. Phys.: Condens. Matter* **15**, S693 (2003).
 [20] Supriyo Datta, *Electronic Transport in Mesoscopic Systems* (Cambridge University Press, Cambridge, 1995).
 [21] Branislav K. Nikolić, Satofumi Souma, Liviu P. Zârbo, and Jairo Sinova, *Phys. Rev. Lett.* **95**, 046601 (2005).
 [22] Branislav K. Nikolić, Liviu P. Zârbo, and Satofumi Souma, *Phys. Rev. B* **73**, 075303 (2006).
 [23] Giuseppe Grosso and Giuseppe Pastori Parravicini, *Solid State Physics*, Academic Press (2000).
 [24] C. L. Kane and E. J. Mele, *Phys. Rev. Lett.* **95**, 146802 (2005).
 [25] J. C. Slater and G. F. Koster, *Phys. Rev.* **94**, 1498 (1954).
 [26] L. Petersen and P. Hedegård, *Surf. Sci.* **459**, 49 (2000).
 [27] For a basic introduction to the nonequilibrium Green's function formalism, see Ref. 20. The LKF is briefly summarized in Ref. 21, and is introduced in some detail in Ref. 22.
 [28] Ming-Hao Liu, Son-Hsien Chen, and Ching-Ray Chang, arXiv:0802.0366v2.
 [29] Charles Kittel, *Introduction to Solid State Physics*, 8th ed. (Wiley, 2005).
 [30] J. J. Sakurai, *Modern Quantum Mechanics*, revised ed. (Addison-Welsey, New York, 1994).
 [31] Ming-Hao Liu, Kuo-Wei Chen, Son-Hsien Chen, and Ching-Ray Chang, *Phys. Rev. B* **74**, 235322 (2006).
 [32] Mathias Bode, *Rep. Progr. Phys.* **66**, 523 (2003).